ELSEVIER

Journal of Organometallic Chemistry 655 (2002) 218–226

Journal of Organometallic Chemistry

www.elsevier.com/locate/jorganchem

Dimethylplatinum(II) and tetramethylplatinum(IV) complexes of 1-methyl-(2-alkylthiomethyl)-1*H*-benzimidazoles: experimental and DFT-calculated structures and NMR spectra

Axel Knödler [a], Wolfgang Kaim [a,*], Vimal K. Jain [b], Stanislav Záliš [c]

[a] *Institut für Anorganische Chemie, Universität Stuttgart, Pfaffenwaldring 55, D-70550 Stuttgart, Germany*
[b] *Novel Materials and Structural Chemistry Divsion, Bhabha Atomic Research Centre, Mumbai 400 085, India*
[c] *J. Heyrovsky Institute of Physical Chemistry, Academy of Sciences of the Czech Republic, Dolejškova 3, CZ-18223 Prague, Czech Republic*

Received 24 January 2002; accepted 15 April 2002

Abstract

The compounds (L)$PtMe_n$ where $n = 2$ or 4 and L = mmb (1-methyl-(2-methylthiomethyl)-1*H*-benzimidazole) or L = mtb (1-methyl-(2-*tert*-butylthiomethyl)-1*H*-benzimidazole) were characterized by X-ray crystallography (except for (mtb)$PtMe_2$) and by ^{1}H- and ^{195}Pt-NMR spectroscopy. The tetramethylplatinum(IV) complexes exhibit a variable degree of dynamic ^{1}H-NMR behavior due to the mobility at the thioether sulfur atom in the non-planar five-membered chelate ring, as supported by structural analysis. Density-functional theory (DFT) calculations were used to reproduce the structural features and the ^{1}H-NMR chemical shifts. In comparison with other late transition metal complexes of these N–S chelate ligands the Me_4Pt and especially the Me_2Pt compounds exhibit a relatively stronger preference of the metal for the sulfur donor.

Keywords: Benzimidazole ligands; Crystal structures; NMR spectroscopy; Platinum compounds; Thioether ligands

1. Introduction

1-Methyl-(2-alkylthiomethyl)-1*H*-benzimidazoles are bidentate N–S-chelate ligands, which combine the imine-binding site of the amino acid histidine with the thioether function of methionine [1,2]. A number of structurally analyzed complexes of mmb = 1-methyl-(2-methylthiomethyl)-1*H*-benzimidazole and mtb = 1-methyl-(2-*tert*-butylthiomethyl)-1*H*-benzimidazole with Cu^I [3,4], Cu^{II} [3], Ag^I [5], Au^I [6], Re^I [7], Rh^{III} and Ir^{III} [8] has been reported, typically involving the formation of five-membered chelate rings. However, the $(PPh_3)Au^+$ fragment was found to coordinate exclusively through the imine nitrogen function [6].

With Cu^+ ions two mmb ligands form an unusual complex cation $[Cu(mmb)_2]^+$ with a sawhorse structure which, remarkably, undergoes an electrochemically completely reversible oxidation to the copper(II) form [4]. A rather small geometry change between the two forms is held responsible for this observation. Furthermore, copper complexes with mmb or mtb and *ortho*-quinone ligands Q exhibit the rarely observed [9] phenomenon of valence tautomerism (redox isomerism, (1)) [1,2].

$$(Q^{2-})Cu^{II}(mmb) \rightleftharpoons (Q^{\bullet -})Cu^{I}(mmb) \quad (1)$$

Such behavior had previously been observed only for amine oxidase enzymes [10].

In the following we shall describe the NMR spectroscopic and (in part) structural characterization of the compounds (L)$PtMe_n$ where $n = 2$ or 4 and L = mmb or mtb. Both organoplatinum complex fragments are electron rich, either through the d^8 configuration of Pt^{II} or through the tetraalkyl substitution at Pt^{IV} [11]; however, they also stabilize anion radical ligands [11,12]. With α-diimine (1,4-diaza-1,3-butadiene) ligands the tetramethylplatinum(IV) compounds exhibit an unusual excited state chemistry with low-lying σ(Pt–C)-to-π*(α-diimine) charge transfer transitions and photoinduced

* Corresponding author. Tel.: +49-711-685-4170/71; fax: +49-711-685-4165.
E-mail address: kaim@iac.uni-stuttgart.de (W. Kaim).

0022-328X/02/$ - see front matter
PII: S0022-328X(02)01564-4

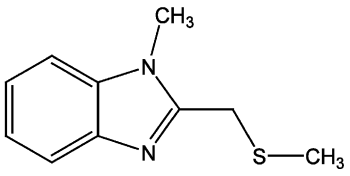

mmb

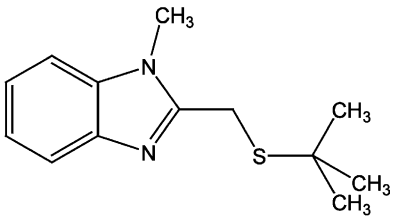

mtb

Pt–C bond homolysis [11,12]. A review on organometallic platinum(IV) compounds is available [13].

2. Results and discussion

2.1. Synthesis and structures

The colorless compounds (L)PtMe$_n$ were obtained from the corresponding N–S ligands [1–8] and the precursors (μ-SMe$_2$)Pt$_2$Me$_m$, m = 4 or 8 [14,15]. Complexes (mmb)PtMe$_2$ and (L)PtMe$_4$, L = mmb, mtb, could be structurally characterized after crystallization from acetone, the results are summarized in Tables 1–3 and the molecular structures illustrated through Figs. 1–3. No unusual intermolecular interactions were observed (Fig. 4).

The compounds exhibit the anticipated chelate arrangement with non-planar five-membered rings NCCSPt (envelope conformation). Relative to a MCCN best plane the deviation for the sulfur atom is 0.6858 Å for (mmb)PtMe$_2$, 0.7846 Å for (mmb)PtMe$_4$ and 0.6518 for (mtb)PtMe$_4$. As a consequence, all four methyl groups are distinctly different for the Me$_4$Pt

Table 1
Crystallographic data and refinement parameters [a]

	Me$_2$Pt(mtb)	Me$_4$Pt(mmb)	Me$_4$Pt(mtb)
Empirical formula	$C_{15}H_{24}N_2PtS$	$C_{14}H_{24}N_2PtS$	$C_{17}H_{30}N_2PtS$
Formula weight	459.51	447.50	489.58
Crystal size (mm)	0.2 × 0.2 × 0.15	0.2 × 0.15 × 0.15	0.2 × 0.2 × 0.2
Diffractometer	Siemens P3	NONIUS KAPPA CCD	Siemens P3
Temperature (K)	173(2)	298(2)	173(2)
Crystal system	Monoclinic	Monoclinic	Monoclinic
Space group	$P2_1/n$	$P2_1/c$	$P2_1/n$
Unit cell dimensions			
a (Å)	12.392(2)	8.1931(2)	9.505(2)
b (Å)	8.987(3)	13.3909(3)	18.641(4)
c (Å)	15.247(3)	14.9743(4)	10.959(2)
β (°)	106.14(3)	97.528(1)	105.81(3)
V (Å^3)	1631.1(7)	1628.72(7)	1868.2(6)
Z	4	4	4
D_{calc} (g cm^{-3})	1.871	1.825	1.741
Absorption coefficient (cm^{-1})	0.8720	0.8730	0.7619
2θ Range (°)	2.66–24.10	3.10–27.48	2.19–30.00
Index ranges	$-14 \le h \le 13$, $0 \le k \le 10$, $0 \le l \le 17$	$-10 \le h \le 10$, $-17 \le k \le 16$, $-19 \le l \le 19$	$-12 \le h \le 13$, $-5 \le k \le 26$, $-15 \le l \le 15$
Reflections collected	6311	27001	6716
Number of unique reflections	2563	3719	5459
Absorption correction	DIFABS [30]	HABITUS [31]	
GOF (F^2) [b]	1.030	1.140	1.199
Data/restraints/parameters	2563/0/172	3719/0/164	5459/0/106
R indices (all data) [c,d]	$R_1 = 0.1062$, $wR_2 = 0.2285$	$R_1 = 0.0370$, $wR_2 = 0.0756$	$R_1 = 0.0548$, $wR_2 = 0.0978$
Largest residual densities (e Å^{-3})	2.781/−2.188	2.211/−0.876	1.853/−1.670

[a] Graphite monochromated Mo–K$_\alpha$ radiation ($\lambda = 0.71073$ Å).
[b] GOF = $\{\Sigma\, w(|F_o|^2 - |F_c|^2)^2/(n-m)\}^{1/2}$; n = number of data; m = number of variables.
[c] $R = (\Sigma||F_o| - |F_c||)/\Sigma|F_o|$.
[d] $R_w = \{\Sigma[w(|F_o|^2 - |F_c|^2)^2]/\Sigma[w(F_o^4)]\}^{1/2}$.

Table 2
Selected experimental and calculated bond lengths (Å) and angles (°) for $Me_2Pt(mtb)$

	Experimental	Calculated
Bond lengths		
Pt(1)–C(24)	2.027(8)	2.068
Pt(1)–C(23)	2.064(8)	2.071
Pt(1)–N(1)	2.124(5)	2.130
Pt(1)–S(1)	2.3499(18)	2.351
S(1)–C(9)	1.827(7)	1.858
S(1)–C(10)	1.859(8)	1.904
N(1)–C(8)	1.336(8)	1.331
C(8)–C(9)	1.478(11)	1.492
Bond angles		
C(24)–Pt(1)–C(23)	86.1(4)	84.0
C(24)–Pt(1)–N(1)	96.6(3)	99.0
C(23)–Pt(1)–N(1)	177.3(3)	176.9
C(24)–Pt(1)–S(1)	175.2(2)	171.4
C(23)–Pt(1)–S(1)	94.4(3)	93.6
N(1)–Pt(1)–S(1)	82.92(17)	83.3
C(9)–S(1)–C(10)	103.0(3)	103.8
C(9)–S(1)–Pt(1)	97.4(3)	97.7
C(10)–S(1)–Pt(1)	110.8(2)	112.9

Table 3
Selected experimental and calculated bond lengths (Å) and angles (°) for $Me_4Pt(mmb)$ and $Me_4Pt(mtb)$

	$Me_4Pt(mmb)$		$Me_4Pt(mtb)$	
	Experimental	Calculated	Experimental	Calculated
Bond lengths				
Pt–C(21)	2.162(5)	2.183	2.206(6)	2.194
Pt–C(22)	2.136(5)	2.147	2.226(7)	2.194
Pt–C(23)	2.050(6)	2.071	2.045(6)	2.072
Pt–C(24)	2.064(5)	2.077	2.054(6)	2.074
Pt–N(1)	2.167(4)	2.183	2.165(4)	2.186
Pt–S	2.4188(12)	2.416	2.4433(14)	2.428
S–C(9)	1.810(5)	1.843	1.811(6)	1.826
S–C(10)	1.791(5)	1.827	1.850(6)	1.843
N(1)–C(8)	1.324(6)	1.387	1.320(7)	1.328
C(8)–C(9)	1.484(6)	1.496	1.500(8)	1.495
Bond angles				
C(23)–Pt–C(24)	88.2(2)	87.3	88.9(3)	86.0
C(23)–Pt–C(22)	88.9(2)	88.8	88.9(3)	87.9
C(23)–Pt–C(21)	88.7(2)	87.7	88.6(2)	87.4
C(24)–Pt–C(22)	89.9(3)	91.2	85.8(2)	84.3
C(24)–Pt–C(21)	87.2(3)	86.2	86.8(2)	89.5
C(22)–Pt–C(21)	176.3(2)	175.7	172.3(2)	172.6
C(24)–Pt–N(1)	96.80(19)	96.2	96.4(2)	97.0
C(23)–Pt–N(1)	174.9(2)	175.8	174.6(2)	173.8
C(22)–Pt–N(1)	89.94(18)	90.2	92.1(2)	94.2
C(21)–Pt–N(1)	92.65(18)	93.4	92.05(18)	89.2
C(24)–Pt–S	171.70(19)	170.1	169.29(19)	168.8
C(23)–Pt–S	94.96(18)	94.6	93.16(19)	93.6
C(22)–Pt–S	97.87(18)	98.5	104.72(16)	106.0
C(21)–Pt–S	85.18(16)	84.2	82.71(15)	80.1
N(1)–Pt–S	80.26(10)	81.5	81.49(12)	80.9
C(9)–S–C(10)	99.2(3)	100.3	103.1(3)	103.9
C(9)–S–Pt	96.90(15)	95.9	97.11(18)	97.7
C(10)–S–Pt	110.6(2)	113.3	119.20(19)	114.9

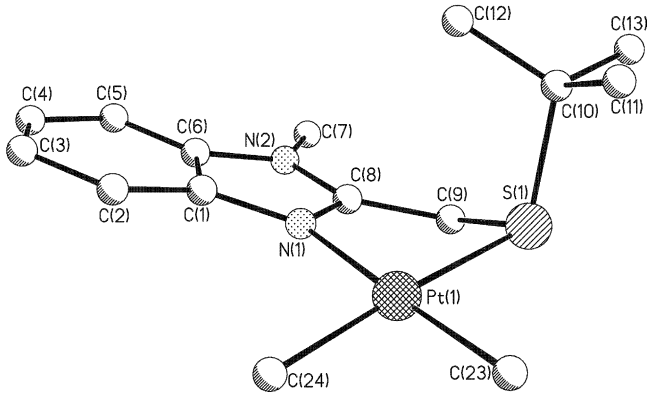

Fig. 1. Molecular structure of $Me_2Pt(mtb)$.

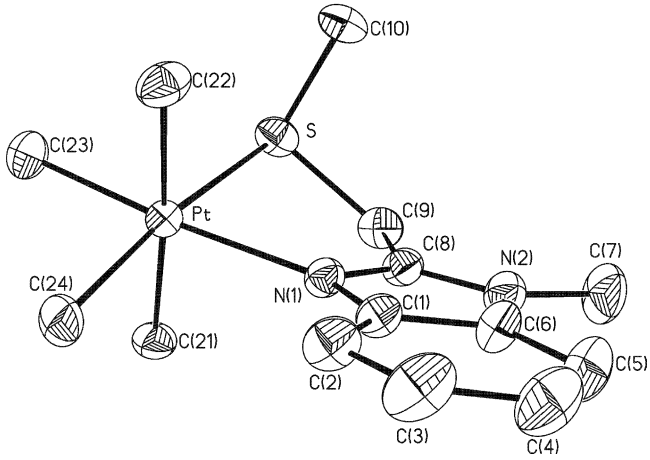

Fig. 2. Molecular structure of $Me_4Pt(mmb)$.

compounds, as confirmed by ^{1}H-NMR spectroscopy (cf. below). Whereas the equatorial methyl groups show a typical *trans* influence in (mmb)$PtMe_2$ with a distinctly longer bond from Pt^{II} to C(23) (*trans* to N) than to C(24) (*trans* to S), there is no such clear effect for the $PtMe_4$ analogues.

The compounds with the $PtMe_4$ complex fragments have longer Pt–C(axial) bonds of >2.13 Å than the 2.05 Å of the Pt–C(equatorial) distances. Such differences were noted previously [11], being attributable to a particularly large bond-lengthening *trans* influence from one formally carbanionic ligand on the other. There is a remarkable variation, however, with the mtb complex having distinctly longer axial Pt–CH_3 bonds. Especially the bond to C(22) is long at 2.226(7) Å, the corresponding methyl ligand is in close contact with the *tert*-butyl group at the sulfur atom (Fig. 3). Accordingly, the corresponding angles C(24)–Pt–C(22) at 85.8° and C(22)–Pt–C(21) at 172.3° deviate most significantly from the 90 or 180° values expected for an ideally octahedral arrangement (Table 3).

The density-functional theory (DFT)-calculated bond parameters for $Me_nPt(mtb)$, $n = 2$ and 4, generally agree with the experimental structures (Tables 2 and 3). There

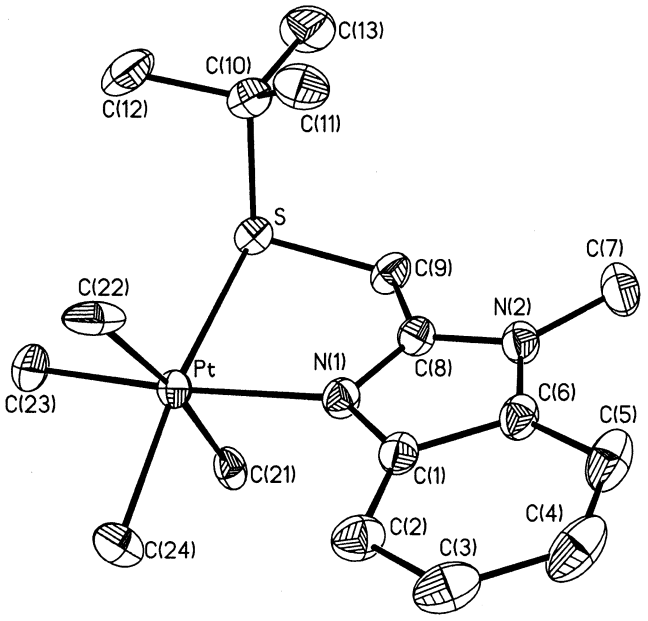

Fig. 3. Molecular structure of $Me_4Pt(mtb)$.

are slight discrepancies for some parameters involving the sulfur atom, which suggests a particular structural sensitivity around that center. In addition, the difference between (short) equatorial and (long) axial Pt–methyl bonds is calculated smaller (0.12 Å) than actually observed at ca. 0.165 Å, mainly due to an overestimation of the equatorial bond lengths.

The three new structurally characterized compounds invite comparison with other transition metal complexes of the mmb and mtb ligands [3–8]. The differences Δd between the M–N and M–S distances in the chelate rings are particularly revealing, reflecting the different affinities of the metals in their respective oxidation states to the imine nitrogen center or to the 'softer' thioether sulfur donor atom. Table 4 lists the data available.

The sequence in Table 4 as summarized in (2) for Δd shows that the organoplatinum species exhibit a comparatively high affinity to the thioether sulfur, the low-valent Me_2Pt^{II} system even more so than the Pt^{IV} species.

$$Pt^{II} < Os^{II} < Pt^{IV} < Ir^{III} < Rh^{III} < Re^{I} < Cu^{I} < Ag^{I} < Cu^{II} \quad (2)$$

As a general rule, complexes of the heavier homologues and with lower metal oxidation states exhibit smaller Δd values, i.e. an increasing affinity towards the sulfur donor.

2.2. NMR spectroscopy

2.2.1. Platinum(II) complexes

Coordination of Me_2Pt to the N–S ligands causes the expected low-field shift of the ^{1}H-NMR resonances [3–8], the data are summarized in Table 5.

Remarkably, the methylene protons in the chelate ring next to the alkylsulfur center are equivalent at ambient temperatures for both the mmb and mtb compounds. In view of the crystal structure with a non-planar chelate ring this observation suggests a rapid interconversion of conformers due to little steric hindrance from the d^8 metal environment. The situation is different for d^6 metal complexes such as $Cl(OC)_3Re^{I}$(mmb), $Cl(OC)_3Re^{I}$(mtb), $[Cl(Cym)Os^{II}$(mmb)$]^+$, $[Cl(Cym)Os^{II}$(mtb)$]^+$ [7] or the tetramethylplatinum(IV) species described below; efficient back donation from platinum(II) to acceptor orbitals at the sulfur atom may also help to lower the inversion barrier considerably.

The DFT-calculated ^{1}H-NMR chemical shifts for Me_2Pt(mtb) are in good agreement with the experiment (cf. Table 7); except for the methylene protons adjacent to the sulfur atom the calculated values are slightly higher than the measured ones. The shift difference between both methyl groups is also reproduced reasonably well.

Protons close to the metal exhibit coupling with the ^{195}Pt isotope (33.8%, $I = 1/2$). The methyl groups are distinctly different in that the signal at lower field (i.e. *trans* to N) exhibits a smaller ^2J(Pt–H) coupling constant, in agreement with previous results [11,12,16]. The ^3J(Pt–H) coupling constants of the methylene or methylthio groups are rather small and are comparable to reported data [17].

The ^{195}Pt-NMR spectra yield chemical shifts of −3770 ppm for Me_2Pt(mmb) and −3831 ppm for Me_2Pt(mtb). Both the range of the shift for dialkylplatinum(II) species [18] and the slightly more negative value for the more electron rich system are as expected.

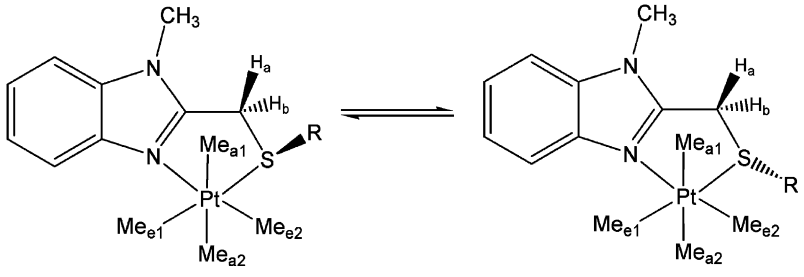

Fig. 4. Inversion at the sulfur atom in Me_4Pt(mmb) and Me_4Pt(mtb).

Table 4
Comparison of structural data for complexes with mmb and mtb

Complex	$\Delta d = d(M-S) - d(M-N)$	Angle C–S–C (ligand)	Bite angle N–M–S	Reference
[(mtb)$PtMe_2$]	0.226	103.0 (3)	82.92 (17)	this work
[(mmb)OsCl(Cym)](PF_6)	0.247	98.59 (160)	79.73 (57)	[7]
[(mmb)$PtMe_4$]	0.252	99.2 (3)	80.26 (10)	this work
[(mmb)IrCl(η^5-C_5Me_5)](PF_6)	0.264	99.4 (3)	80.75 (7)	[8]
[(mtb)$PtMe_4$]	0.280	103.1 (3)	81.52 (14)	this work
[(mtb)IrCl(η^5-C_5Me_5)](PF_6)	0.286	103.3 (3)	80.9 (1)	[8]
[(mmb)$AgPO_2F_2$]	0.300 [a]	102.1 (2)	[a]	[5]
[(mmb)RhCl(η^5-C_5Me_5)](PF_6)	0.305	100.5 (3)	80.0 (1)	[8]
[(mtb)RhCl(η^5-C_5Me_5)](PF_6)	0.307	103.2 (2)	80.3 (2)	[8]
[(mtb)$Re(CO)_3Cl$]	0.308	102.6 (3)	79.26 (12)	[7]
[(mmb)$Re(CO)_3Cl$]	0.321	99.3 (4)	78.30 (14)	[7]
[(mmb)$Cu(PPh_3)_2$](BF_4)	0.394	100.9 (3)	84.3 (1)	[3]
[(mtb)$_2$Ag](PF_6)	0.483; 0.432	104.5 (2); 103.7 (2)	77.40 (8); 77.75 (8)	[5]
[(mmb)$_2$Ag](PF_6)	0.483	99.8 (2)	76.17 (6)	[5]
[(mmb)$_2$Cu(η^1-ClO_4)](ClO_4)	0.501; 0.470	99.9 (2); 99.0 (3)	83.1 (1); 83.6 (1)	[3]
[(mmb)$_2$Cu](BF_4)	0.702 [b]	100.7 (1)	82.47 (6)	[4]
[(mmb)Au(PPh_3)](PF_6)	0.948 [c]; 0.941	102.7 (5); 102.4 (4)	[c]	[6]

[a] No chelate ring, but coordination of N and S to different Ag atoms.
[b] 2+2-coordination.
[c] No S-coordination.

Table 5
^{1}H-NMR-data of Me_2Pt(mmb) and Me_2Pt(mtb) [a]

	Me_2Pt(mmb)	Me_2Pt(mtb)
Pt–C(24)H_3	0.54 (3H, ^2J(Pt–H) = 90.4 Hz)	0.59 (3H, ^2J(Pt–H) = 89.3 Hz)
Pt–C(23)H_3	1.02 (3H, ^2J(Pt–H) = 87.9 Hz)	1.03 (3H, ^2J(Pt–H) = 88.6 Hz)
S–CH_3	2.43 (3H, ^3J(Pt–H) = 28.0 Hz)	
S–^{t}Bu		1.24 (s, 3H)
N–CH_3	3.95 (s, 3H)	4.02 (s, 3H)
CH_2–S	4.40 (2H, ^3J(Pt–H) = 9.4 Hz)	4.29 (s, 2H)
C(3,4)H	7.25–7.36 (m, 2H)	7.26–7.31 (m, 2H)
C(5)H	7.53–7.58 (m, 1H)	7.53–7,57 (m, 1H)
C(2)H	8.03–8.09 (m, 1H)	8.03–8.07 (m, 1H)

[a] In acetone-d_6, chemical shifts δ in ppm.

2.2.2. Platinum(IV) complexes

The coordination of Me_4Pt to the N–S ligands causes some significant changes of the ^{1}H-NMR spectra (Table 6).

First, there are two additional ^{195}Pt-split signals for the axial methyl groups at higher field. The ^2J(Pt–H) coupling is much smaller for these resonances due to the strong *trans* influence of alkyl groups on each other in the axial position [11,12,19,20]. The DFT-calculated ^{1}H-NMR chemical shifts for Me_4Pt(mtb) agree reasonably with the experiment (Table 7), especially placing the axial methyl proton resonances at higher field.

For Me_4Pt(mtb) this effect could only be observed at lowered temperatures (233 K) because the chelate ring with the *tert*-butyl-sulfur group inducing non-equivalence at the axial methyl groups shows sufficient mobility to cause line broadening with coalescence at about 280 K (Fig. 5). Variable temperature ^{1}H-NMR also reveals non-equivalence (and coalescence at about 280 K for Me_4Pt(mtb)) of the methylene protons in the chelate ring next to the alkylsulfur center (Fig. 6). Related dynamic phenomena involving inversion at tricoordinate sulfur (Fig. 4) bonded to organoplatinum fragments have been observed before using NMR spectroscopy [21–23].

Table 6
^{1}H-NMR-data of Me_4Pt(mmb) and Me_4Pt(mtb) [a]

	Me_4Pt(mmb) [b]	Me_4Pt(mtb) [c]
Pt–C(21)H_3	−0.37 (3H, ^2J(Pt–H) = 41.7 Hz)	−0.35 (3H, ^2J(Pt–H) = 41.1 Hz)
Pt–C(22)H_3	−0.08 (3H, ^2J(Pt–H) = 44.0 Hz)	0.24 (3H, ^2J(Pt–H) = 44.9 Hz)
Pt–C(24)H_3	0.65 (3H, ^2J(Pt–H) = 75.3 Hz)	0.66 (3H, ^2J(Pt–H) = 74.0 Hz)
Pt–C(23)H_3	1.30 (3H, ^2J(Pt–H) = 74.9 Hz)	1.29 (3H, ^2J(Pt–H) = 75.1 Hz)
CH_3	2.25 (3H, ^3J(Pt–H) = 12.7 Hz)	
^{t}Bu		1.24 (s, 3H)
N–CH_3	3.98 (s, 3H)	4.09 (s, 3H)
CH_2–S	4.42 (AB-System, $^2J_{AB}$ = 11.0 Hz, 4.54 ^3J(Pt–H) = 8.7 Hz)	4.27 (AB-System, $^2J_{AB}$ = 17.9 Hz, 4.56 ^3J(Pt–H) = 7.4 Hz)
C(3,4)H	7.28–7.33 (m, 2H)	7.27–7.35 (m, 2H)
C(5)H	7.55–7.58 (m, 1H)	7.56–7.60 (m, 1H)
C(2)H	7.80–7.83 (m, 1H)	7.80–7.82 (m, 1H)

[a] In acetone-d_6, chemical shifts δ in ppm.
[b] At room temperature.
[c] At 233 K.

Table 7
Comparison of experimental and DFT calculated ^{1}H-NMR chemical shifts (ppm) of $Me_4Pt(mtb)$ and $Me_2Pt(mtb)$

	$Me_4Pt(mtb)$		$Me_2Pt(mtb)$	
	Experimental [a]	Calculated	Experimental [b]	Calculated
Pt–CH_3 (ax)	−0.35, 0.24	0.45		
Pt–C(24)H_3	0.66	1.27	0.59	0.70
Pt–C(23)H_3	1.29	2.08	1.03	1.51
^{t}Bu	1.24	1.75	1.24	1.52
N–CH_3	4.09	3.98	4.02	4.12
CH_2–S	4.27, 4.56	4.36	4.29	4.07
C*H*	7.27–7.35 (m, 2H)	7.51	7.26–7.31 (m, 2H)	7.80
C*H*	7.56–7.60 (m, 1H)	7.55	7.53–7.57 (m, 1H)	8.03
C*H*	7.80–7.82 (m, 1H)	8.55	8.03–8.07 (m, 1H)	9.17

[a] At 233 K in acetone-d_6.
[b] At room temperature in acetone-d_6.

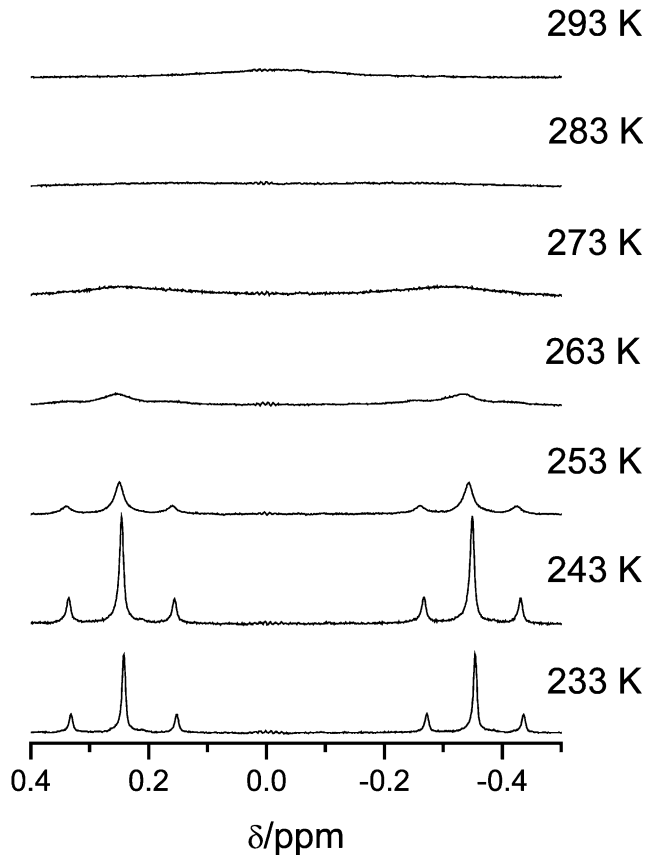

Fig. 5. Temperature dependence of the signals for the axial Pt–CH_3 protons in the ^{1}H-NMR spectrum of $Me_4Pt(mtb)$ in acetone-d_6.

From the coalescence temperature and the frequency differences of 74.3 Hz between the CH_2 signals or the 149.0 Hz between the resonances of the axial methyl

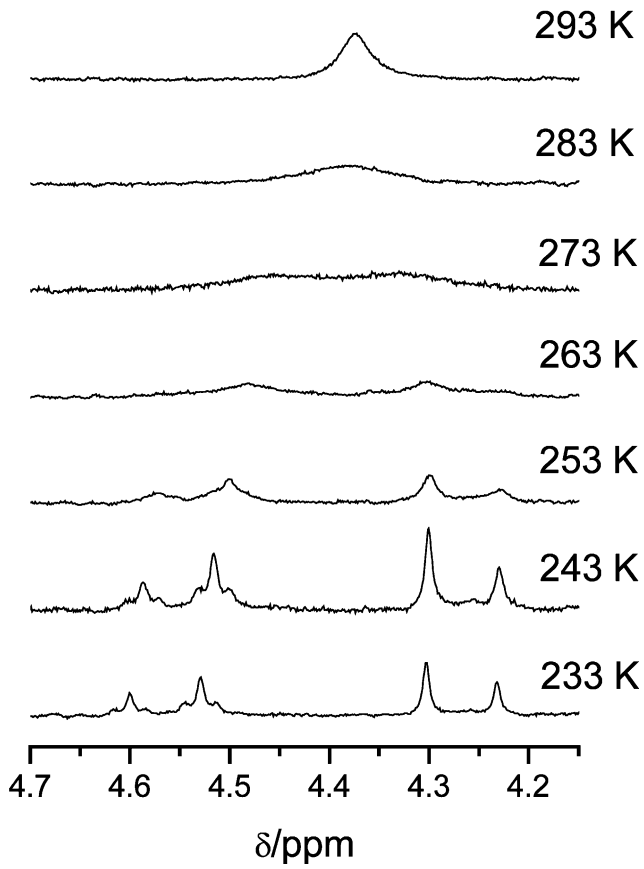

Fig. 6. Temperature dependence of the methylene proton signals in the ^{1}H-NMR spectrum of $Me_4Pt(mtb)$ in acetone-d_6.

groups one can estimate $\Delta G^{\ddagger}$ values of about 57 kJ mol^{-1} according to $\Delta G^{\ddagger} = T_c\ (22.96 + \ln(T_c/\delta\nu))$ (J mol^{-1}) [24]. The unsymmetrical appearance of Fig. 6 with platinum coupling only at the low-field side is conspicuous; according to Karplus-type correlations for spin–spin coupling one may expect H_a to exhibit a larger coupling with ^{195}Pt than H_b.

For the $Me_4Pt(mmb)$ species there is no averaging apparent at room temperature or below, suggesting a distinctly higher activation barrier to the interconversion of conformers. Whereas the hexacoordination at the metal contributes to raise that barrier (as in complexes $Cl(OC)_3Re(mmb)$, $Cl(OC)_3Re(mtb)$, $[Cl(Cym)Os(mmb)]^+$ and $[Cl(Cym)Os(mtb)]^+$ [7]), the introduction of a *tert*-butyl group at sulfur seems to lower that barrier because of steric hindrance which pushes the structure closer to 120° angles (e.g. of C(10)–S–Pt from 110.6° for the mmb complex to 119.2° for the mtb analogue) required in the transition state [25]. Another special feature of $Me_4Pt(mtb)$ is the low-field shift for one particular axial methyl group, which is likely to be the one with C(22), interacting strongly with the *tert*-butyl substituent (cf. Fig. 3).

The smaller ^2J(Pt–H) coupling for the equatorial methyl groups in the tetramethylplatinum compounds relative to the Me_2Pt analogues can be attributed to the

lower s orbital contribution to the Pt–C bonds from d^2sp^3 hybridized Pt^{IV} versus dsp^2-hybridized Pt^{II} [26,27].

The ^{195}Pt-NMR spectra yield chemical shifts of −3053 ppm for Me_4Pt(mmb) and −1786 ppm for Me_4Pt(mtb). Both compounds show the typical [18] shift in comparison to the platinum(II) analogues, however, the distinctly less negative value for Me_4Pt(mtb) remains puzzling since the exchange Me/*tert*-Bu does not normally cause strong shift differences [28]. We tentatively attribute this large chemical shift difference to the significant distortion at the metal in Me_4Pt(mtb) with a lengthened bond Pt–C(22) of 2.226 Å and a decreased angle C(24)–Pt–C(22) of 85.8°.

2.3. Infrared spectroscopy

Two Pt–C(Me) stretching vibrations are observed for the dimethylplatinum complexes (Table 8). The band at higher energy is assigned to the bond vibration in *trans* position to the thioether sulfur donor, involving the shorter bond Pt–C(24). Similar values were reported for thioether complexes of the Me_2Pt fragment [19].

The tetramethylplatinum compounds exhibit essentially the same bands from Pt–C(Me) stretching vibrations with the addition of a more intense band at lower energies. The latter is interpreted as the asymmetric combination from the coupled [19] stretching vibrations involving the *trans*-oriented axial methyl groups. The strong *trans* influence of the methyl ligands causes the low-frequency shift, the symmetrical combination of probably low intensity could not be observed.

2.4. Absorption spectroscopy, cyclic voltammetry

In accordance with the weak acceptor characteristics of 1-methyl-(2-alkylthiomethyl)-1*H*-benzimidazoles [3–8] the complexes do not exhibit metal-to-ligand charge transfer absorptions in the visible or near UV and no reversible reduction in the available electrochemical potential range of > -2.5 V versus ferrocenium/ferrocene. Irreversible oxidation was observed between 0.3 and 0.5 V versus $[Fe(C_5H_5)_2]^{+/0}$ as similarly reported before [11].

Table 8
Stretching frequencies ν_{Pt-C} of complexes [a]

	ν(Pt–C(24))	ν(Pt–C(23))	ν_{as}(Pt–C_2^{ax})
Me_2Pt(mmb)	566	516	
Me_2Pt(mtb)	567	509	
Me_4Pt(mmb)	565	511	480
Me_4Pt(mtb)	566	508	469

[a] Frequencies ν in cm^{-1}(in KBr).

3. Experimental

3.1. Syntheses

3.1.1. Dimethyl(1-methyl-(2-methylthiomethyl)-1H-benzimidazole)platinum(II) Me_2Pt(mmb)

A solution of 78.2 mg (0.136 mmol) $Pt_2Me_4(\mu\text{-}SMe_2)_2$ [14] and 52.3 mg (0.272 mmol) mmb [1,2] in 25 ml diethyl ether was stirred for 15 h at ambient temperature. After removal of half of the solvent the colorless precipitate was filtered, washed with petrol ether and dried under vacuum to yield 81.8 mg (72%). Calc. for $C_{12}H_{18}N_2PtS$ (417.44): C, 34.53; H, 4.35; N, 6.71. Found: C, 34.15; H, 4.57; N, 6.09%. UV–vis (CH_2Cl_2): λ_{max} (ε) = 277 (7900), 284 (7300) nm (M^{-1} cm^{-1}). For NMR and IR data see Tables 5 and 8 and text.

3.1.2. Dimethyl(1-methyl-(2-tert-butylthiomethyl)-1H-benzimidazole)platinum(II) Me_2Pt(mtb)

The above procedure was followed with 68.5 mg (0.119 mmol) $Pt_2Me_4(\mu\text{-}SMe_2)_2$ and 55.8 mg (0.238 mmol) mtb [5,8] to yield 65.6 mg (60%). Calc. for $C_{15}H_{24}N_2PtS$ (459.52): C, 39.21; H, 5.26; N, 6.10. Found: C, 39.28; H, 5.22; N, 5.83%. UV–vis (CH_2Cl_2): λ_{max} (ε) = 277 (6900), 285 (6500) nm (M^{-1} cm^{-1}). For NMR and IR data see Tables 5 and 8 and text.

3.1.3. Tetramethyl(1-methyl-(2-methylthiomethyl)-1H-benzimidazole)platinum(IV) Me_4Pt(mmb)

A solution of 256.0 mg (0.403 mmol) $Pt_2Me_8(\mu\text{-}SMe_2)_2$ [15] and 155.1 mg (0.806 mmol) mmb in 25 ml diethyl ether was stirred for 15 h at ambient temperature. After removal of half of the solvent the solution was kept at −18 °C for 24 h, the colorless precipitate was filtered, washed with petrol ether and dried under vacuum to yield 250.0 mg (69%). Calc. for $C_{14}H_{24}N_2PtS$ (447.51): C, 37.58; H, 5.41; N, 6.26. Found: C, 37.18; H, 5.38; N, 6.08%. UV–vis (CH_2Cl_2): λ_{max} (ε) = 278 (10 000), 286 (8500) nm (M^{-1} cm^{-1}). For NMR and IR data see Tables 6 and 8 and text.

3.1.4. Tetramethyl(1-methyl-(2-tert-butylthiomethyl)-1H-benzimidazole)platinum(IV) Me_4Pt(mtb)

The above procedure was followed with 147.0 mg (0.464 mmol) $Pt_2Me_8(\mu\text{-}SMe_2)_2$ and 108.8 mg (0.232 mmol) mtb to yield 95.4 mg (42%). Calc. for $C_{17}H_{30}N_2PtS$ (489.59): C, 41.71; H, 6.18; N, 5.72. Found: C, 41.58; H, 6.15; N, 5.52%. UV–vis (CH_2Cl_2): λ_{max} (ε) = 277 (10 000), 285 (8700) nm (M^{-1} cm^{-1}). For NMR and IR data see Tables 6 and 8 and text.

3.2. Instrumentation

^{1}H-NMR spectra were taken on a Bruker AC 250 spectrometer, ^{195}Pt-NMR spectra were recorded on a Bruker DPX-300 system with Na_2PtCl_6 in D_2O as external reference. Infrared spectra were obtained using a Perkin–Elmer Paragon 1000 PC instrument. UV–vis/NIR absorption spectra were recorded on a Bruins Instruments Omega 10 spectrophotometer. Cyclic voltammetry was carried out in CH_2Cl_2–0.1 M Bu_4NPF_6 solutions using a three-electrode configuration (glassy carbon working electrode, Pt counter electrode, Ag | AgCl reference) and a PAR 273 potentiostat and function generator. The ferrocene/ferrocenium couple served as internal reference.

3.3. Crystallography

The structures of the compounds were solved through direct methods. The refinement was carried out employing the full matrix least-squares method [29]. All non-hydrogen atoms were refined anisotropically. The hydrogen atoms were introduced at proper geometric positions and treated according to the riding model with isotropic thermal parameters fixed at 20% greater than that of the bonded atom. Anisotropic thermal parameters were refined for all non-hydrogen atoms.

3.4. DFT calculations

Ground state electronic structure calculations of both complexes have been done by DFT methods using the ADF2000.02 [32,33] program package. Within the ADF program, Slater type orbital (STO) basis sets of triple-ζ quality with polarization functions were employed for the Pt and S atoms and double-ζ with polarization functions for the rest of the systems. The inner shells were represented by the frozen core approximation; 1s for C, N, 1s–2p for S and 1s–4d for Pt were kept frozen. The following density functionals were used within ADF: the local density approximation (LDA) with VWN parameterization of electron gas data and functional including Becke's gradient correction [34] to the local exchange expression in conjunction with Perdew's gradient correction [35] to the LDA expression. The scalar relativistic (SR) zero order regular approximation (ZORA) was used for geometry optimization.

The calculations of NMR shielding tensors were done by a separate program using Kohn–Sham orbitals from single point calculations at optimized geometries. The integration accuracy in ADF was set to the recommended value 6 (which means significant digits by which an internal set of standard integrals must be evaluated). The calculations of NMR shielding tensors within ADF were based on a SR Pauli-type Hamiltonian using gauge, including atomic orbitals [36,37]. The expressions for evaluating the NMR shielding tensor and performance of the method for simple Pt complexes can be found in [38]. The calculated chemical shifts were expressed as a difference between the shielding of the reference (TMS) and the complex of interest using the same basis set and functionals for both systems.

4. Supplementary material

Crystallographic data for the structural analysis have been deposited with the Cambridge Crystallographic Data Centre, CCDC nos. 175715, 175716 and 175717. Copies of the information may be obtained free of charge from The Director, CCDC, 12 Union Road, Cambridge CB2 1EZ, UK (Fax: +44-1223-336033; e-mail: deposit@ccdc.cam.ac.uk or www: http://www.ccdc.cam.ac.uk).

Acknowledgements

Support from the Deutsche Forschungsgemeinschaft (Bonn; Graduiertenkolleg 'Magnetische Resonanz'), the BMBF (Berlin; project IND 99/060), the FCI (Frankfurt am Main), the Ministry of Education of the Czech Republic and the DLR (Bonn; KONTAKT project CZE 00013) is gratefully acknowledged.

References

[1] J. Rall, E. Waldhör, B. Schwederski, M. Schwach, S. Kohlmann, W. Kaim, in: A.X. Trautwein (Ed.), Bioinorganic Chemistry: Transition Metals in Biology and their Coordination Chemistry, VCH, Weinheim, 1997, p. 476.
[2] (a) J. Rall, M. Wanner, M. Albrecht, F.M. Hornung, W. Kaim, Chem. Eur. J. 5 (1999) 2802;
(b) J. Rall, M. Wanner, M. Albrecht, F.M. Hornung, W. Kaim, J. Bioinorg. Chem. 74 (1999) 187.
[3] M. Albrecht, K. Hübler, T. Scheiring, W. Kaim, Inorg. Chim. Acta 287 (1999) 204.
[4] M. Albrecht, K. Hübler, S. Zalis, W. Kaim, Inorg. Chem. 39 (2000) 4731.
[5] M. Albrecht, K. Hübler, W. Kaim, Z. Anorg. Allg. Chem. 626 (2000) 1033.
[6] M. Albrecht, K. Hübler, W. Kaim, Z. Naturforsch. 54b (1999) 1606.
[7] A. Knödler, M. Wanner, W. Kaim, J. Fiedler, Z. Anorg. Allg. Chem., in press.
[8] M. Albrecht, T. Scheiring, T. Sixt, W. Kaim, J. Organomet. Chem. 596 (2000) 84.
[9] C.G. Pierpont, Coord. Chem. Rev. 216–217 (2001) 99.
[10] D.M. Dooley, M.A. McGuirl, D.E. Brown, P.N. Turowski, W.S. McIntire, P.F. Knowles, Nature (London) 349 (1991) 262.
[11] S. Hasenzahl, H.-D. Hausen, W. Kaim, Chem. Eur. J. 1 (1995) 95.
[12] (a) W. Kaim, A. Klein, S. Hasenzahl, H. Stoll, S. Zalis, J. Fiedler, Organometallics 17 (1998) 237;
(b) A. Klein, S. Hasenzahl, W. Kaim, J. Chem. Soc. Perkin Trans. 2 (1997) 2573.

[13] V.K. Jain, G.S. Rao, L. Jain, Adv. Organomet. Chem. 27 (1987) 113.
[14] J.D. Scott, R.J. Puddephatt, Organometallics 2 (1983) 1643.
[15] M. Lashanizadeghan, M. Rashidi, J.E. Hux, R.J. Puddephatt, S.S.M. Ling, J. Organomet. Chem. 269 (1984) 317.
[16] H.C. Clark, L.E. Manzer, J.E.H. Ward, Can. J. Chem. 52 (1974) 1165.
[17] V.K. Jain, S. Chaudhury, R. Bohra, Polyhedron 12 (1993) 2377.
[18] P.S. Pregosin, Annu. Rev. NMR Spectrosc. 17 (1986) 285.
[19] (a) D.E. Clegg, J.R. Hall, G.A. Swile, J. Organomet. Chem. 36 (1972) 403;
(b) See also D.M. Adams, J. Chatt, B.L. Shaw, J. Chem. Soc. (1960) 2047.
[20] T.G. Appleton, H.C. Clark, L.E. Manzer, Coord. Chem. Rev. 10 (1973) 335.
[21] E.W. Abell, S.K. Bhargava, K.G. Orrell, Prog. Inorg. Chem. 32 (1984) 1.
[22] K.G. Orrell, Coord. Chem. Rev. 96 (1989) 1.
[23] K.G. Orrell, V. Sik, Annu. Rep. NMR Spectrosc. 19 (1987) 79.
[24] H. Günther, Grundlagen, Konzepte und Anwendungen der Protonen und Kohlenstoff-13 Kernresonanz-Spektroskopie in der Chemie, 3. Aufl, Thieme Verlag, Stuttgart, Germany, 1992, p. 310.
[25] E.W. Abel, A.R. Khan, K. Kite, K.G. Orrell, V. Šik, J. Chem. Soc. Dalton Trans. (1980) 1975.
[26] A. Pidcock, R.E. Richards, L.M. Venanzi, J. Chem. Soc. A (1966) 1707.
[27] S. Chattopadhyay, C. Sinha, P. Basu, A. Chakravorty, Organometallics 10 (1991) 1135.
[28] E.W. Abel, I. Moss, K.G. Orrell, V. Šik, D. Stephenson, P.A. Bates, M.B. Hursthouse, J. Chem. Soc. Dalton Trans. (1988) 521.
[29] SHELXTL 5.1, Bruker Analytical X-ray Systems, Madison, Wisconsin, USA, 1998.
[30] N. Walker, D. Stuart, Acta Crystallogr. Sect. A 39 (1983) 158.
[31] STOE&CIE GMBH, X-SHAPE, Crystal Optimisation Program for Numerical Absorption Correction, based on the Program 'HABITUS' by W. Herrendorf, Gießen (Germany) 1995.
[32] C. Fonseca Guerra, J.G. Snijders, G. Te Velde, E.J. Baerends, Theor. Chim. Acc. 99 (1998) 391.
[33] S.J.A. van Gisbergen, J.G. Snijders, E.J. Baerends, Comput. Phys. Commun. 118 (1999) 119.
[34] A.D. Becke, Phys. Rev. A 38 (1988) 3098.
[35] J.P. Perdew, Phys. Rev. A 33 (1986) 8822.
[36] G. Schreckenbach, T. Ziegler, J Phys. Chem. 99 (1995) 606.
[37] G. Schreckenbach, T. Ziegler, Int. J. Quantum Chem. 61 (1997) 899.
[38] T.M. Gilbert, T. Ziegler, J. Phys. Chem. A 103 (1999) 7535.